Photonic band-gap effects and magnetic activity in dielectric composites

2002 J. Phys.: Condens. Matter 14 4035

(http://iopscience.iop.org/0953-8984/14/15/317)

INSTITUTE OF PHYSICS PUBLISHING JOURNAL OF PHYSICS: CONDENSED MATTER

J. Phys.: Condens. Matter **14** (2002) 4035–4044 PII: S0953-8984(02)34267-X

Photonic band-gap effects and magnetic activity in dielectric composites

Stephen O'Brien and John B Pendry

Condensed Matter Theory Group, The Blackett Laboratory, Imperial College, London SW7 2BZ, UK

Received 26 February 2002
Published 4 April 2002
Online at stacks.iop.org/JPhysCM/14/4035

Abstract

We develop an effective medium description of a two-dimensional photonic band-gap medium composed of dielectric cylinders of large dielectric constant. Using the transfer matrix method we have calculated reflection coefficients for a slab of the composite and plane-wave incidence, as well as the (complex) wavevector for the infinite system. From these quantities we derive an effective permittivity and permeability for the composite. In the case of p-polarized incidence the composite displays a negative magnetic permeability at microwave frequencies due to single-scatterer resonances in the medium.

(Some figures in this article are in colour only in the electronic version)

1. Introduction

As a result of theoretical investigations by Veselago [1] and more recently by Pendry [2], there is now a keen interest in the development of so-called left-handed materials (LHM). Veselago's analysis revealed that where the permittivity and permeability were simultaneously negative, the refractive index must also be so. He used the term 'left-handed' as the electric field, magnetic intensity and propagation vector now obey a left-hand rule. Some novel electromagnetic properties can be expected of a LHM. For example, Snell's law now requires refraction toward the same side of the surface normal, rather than to the opposite side, at an interface between materials having opposite signs of refractive index. Rays from a source placed closely to a slab of such a material will come to a focus inside the slab and once more on the opposite side of the slab. In addition, Pendry's analysis demonstrated that the non-propagating near-field components associated with the source would also be present in the image formed with their amplitudes restored, allowing for improved imaging potential beyond the diffraction limit.

An experimental demonstration of a LHM has been given very recently [3,4]. The authors combined two-dimensional arrays of split ring resonators [5] and metallic wires [6], and showed that the resulting meta-material has a negative refractive index in the microwave region of the spectrum. Above the resonance frequency the split rings give rise to a negative effective

permeability, while the interlaced wire arrays act like a high-pass filter with a negative effective permittivity at lower frequencies.

In this paper we propose another structure that is characterized by a negative effective permeability. Rather than using the LC-resonance of the conducting split rings to attain a negative permeability as an average quantity, the mechanism we propose involves the well known Mie resonance in dielectric particles [7]. It is these resonances which give rise to the heavy-photon bands in photonic crystals [8]. These bands are usually considered in a regime where the free-space wavelength of the radiation is of the order of the unit-cell dimension in the crystal. As a result, the concept of an average permeability or permittivity for the system as discussed in [5] is not well defined. In order that we can consider our system as an effective medium, we allow for a large dielectric constant for the inclusions in the composite. In this way the free-space wavelength is much larger than the spacing between inclusions at the resonance frequency. Advances in the manufacture of low-loss ferroelectric materials make the large dielectric constant possible in real materials at microwave frequencies. These materials also have the added advantage of possessing a dielectric constant tunable with the applied voltage.

We consider the case of p-polarized light incident upon a square lattice of cylinders. The magnetic field is oriented parallel to the cylinders and we examine how the presence of the Mie resonance perturbs the band at low energy which has an otherwise linear dispersion.

2. Single-scatterer resonances

There are several differing mechanisms whereby stop bands appear in photonic crystals. One is the extended or macroscopic Bragg resonance, where multiple scattering and interference lead to the formation of gaps in the dispersion. Another arises because of single-scatterer resonances (Mie resonances) in the system. These resonances are the electromagnetic equivalent of the resonant scattering from a potential well in quantum mechanics where, by analogy, scatterers with a dielectric constant larger than that of the surrounding medium constitute an attractive potential for photons.

The origin of the magnetic activity in our system is the zeroth-order TE Mie resonance. For this polarization the displacement current inside the particle in the plane perpendicular to the cylinder axis can be greatly enhanced when the size parameter $x = ka = 2\pi a/\lambda$ is resonant with a natural mode of oscillation of the cylinder. Here a is the cylinder radius, and λ is the wavelength of the incident radiation. The attractive potential in our case will be large, leading to a high-Q resonance and strong confinement of photons inside the cylinders.

The resonant size parameters can be found from the poles of the coefficients of the internal field. For example, in the case of an infinite cylinder, and for a TE-polarized incident plane wave, the magnetic fields are given by

$$H_y^{inc}(kr) = H_0 \sum_m \mathrm{i}^m J_m(kr)\mathrm{e}^{\mathrm{i}m\phi}, \tag{1}$$

$$H_y^{scatt}(kr) = -H_0 \sum_m \mathrm{i}^m a_m H_m^{(1)}(kr)\mathrm{e}^{\mathrm{i}m\phi}, \tag{2}$$

$$H_y^{int}(nkr) = H_0 \sum_m \mathrm{i}^m c_m J_m(nkr)\mathrm{e}^{\mathrm{i}m\phi}, \tag{3}$$

where

$$c_m = \frac{1}{J_m(nx)}[J_m(x) - a_m H_m^{(1)}(x)], \tag{4}$$

$$a_m = \frac{J'_m(nx)J_m(x) - nJ_m(nx)J'_m(x)}{J'_m(nx)H_m^{(1)}(x) - nJ_m(nx)H_m'^{(1)}(x)}. \tag{5}$$

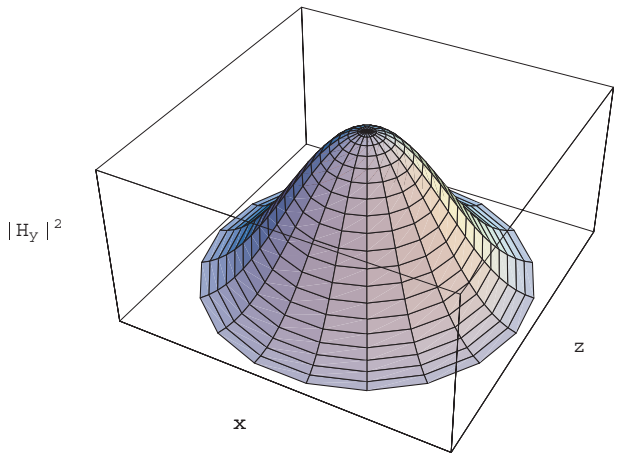

Figure 1. The azimuthally symmetric part of $|\vec{H}_y^{int}|^2$, plotted over the cross-section of the cylinder at the position of the zeroth-order TE Mie resonance.

The electric fields can be found from the magnetic fields using

$$\vec{\nabla} \times \vec{H} = -\mathrm{i}\omega\varepsilon\vec{E} \tag{6}$$

in each region. Here n is the refractive index of the cylinder and ε is the permittivity of the vacuum or of the cylinder as appropriate. J_m is the cylindrical Bessel function of the first kind and $H_m^{(1)}$ is the Hankel function of the first kind. A prime denotes the derivative with respect to the argument. H_0 is the amplitude of the incident magnetic field and H^{inc}, H^{scatt} and H^{int} denote the incident, scattered and internal magnetic fields respectively. These forms satisfy continuity of the tangential components of the total electric and magnetic fields at the surface of the cylinder.

A characteristic equation is obtained by setting the denominator of the a_m-coefficient equal to zero. The solutions of the characteristic equation are complex. When the incident field is at a frequency close to the real part of this solution, one of the c_m-coefficients dominates over the others, and the internal field is described primarily by the basis function associated with that coefficient. For the zeroth-order resonance only the azimuthally directed displacement current is enhanced and results in an enhanced magnetic field along the cylinder axis. In figure 1 we have plotted the square modulus of the resonant contribution to the magnetic field over the cross-section of the cylinder. In an array of identical cylinders these localized magnetic modes could give rise to a macroscopic bulk magnetization in the system, and hence a non-zero magnetic susceptibility on average.

3. Determination of the effective permittivity and permeability

We wish to characterize the electromagnetic properties of the system in terms of an effective permittivity, ε_{eff}, and an effective permeability, μ_{eff}. One way to obtain these quantities is to perform an averaging of the microscopic fields over a unit cell of the system [5, 9]. Another is to first calculate an effective wave impedance, Z_{eff}, for the system by considering an emergent quantity such as the (complex) reflection coefficient. A suitably defined refractive index for the system then allows the desired quantities to be determined. A similar scheme has been used to derive the effective permittivity and permeability of metallo-dielectric photonic crystals [10]. Figure 2 shows the geometry of our calculation where we have indicated the oscillatory displacement currents, j_D, in the plane of incidence which give rise to the magnetic moment of figure 1.

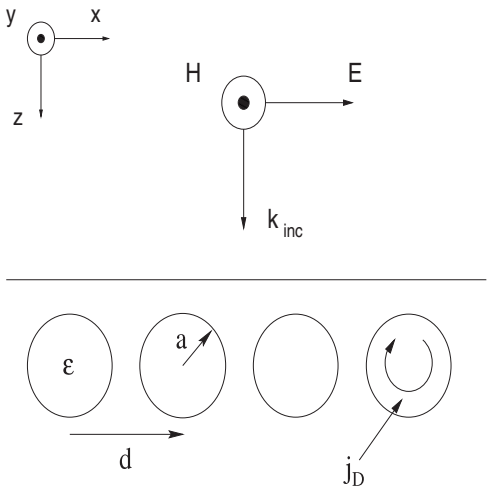

Figure 2. The geometry of the problem. The incident field propagates in the z-direction. The cylinders have radius a, their centre-to-centre spacing is d and the permittivity of the cylinders is ε. We have also illustrated here the resonant displacement currents in the cylinders, j_D, where the magnetic activity that we consider has its origin.

In our case the effective refractive index is calculated on the basis of photonic band-structure calculations. The transfer matrix eigenvalues for the unit cell of our system provide the photonic band structure. In replacing our micro-structured system by an effective homogeneous medium we assume that a single pair of Bloch waves (for each polarization) with wavevectors $\pm\beta$ dominate the band structure in the sense that they present the smallest attenuation having the smallest imaginary part [11]. For normally incident light we can then define

$$\beta = n_{eff} k_{inc}, \tag{7}$$

where $k_{inc} = \omega_{inc}/c_0$ is the wavevector in vacuum. Note that in order that this wavevector describes a decaying wave in the stop-band region we must chose β such that $\mathrm{Im}\{n_{eff}\} \geqslant 0$.

We determine the effective wave impedance for the composite by calculating the coefficient of reflection from a slab. The reflection coefficient is calculated for a monolayer of cylinders and then those for two, four etc layers are calculated using the layer-doubling method [12]. Of course, our effective response functions should be independent of the number of layers present when calculating the reflection coefficient. In the presence of some damping in the dielectric constant of the cylinders, this will be the case after sufficiently many layer doublings. Physically this results in the damping out of the Fabry–Perot resonances of the slab at the frequencies of interest. For such a regime we are justified in equating our complex reflection coefficient, $\tilde{r}$, to the expression for reflection at a plane interface rather than at a plane slab. For normal incidence this expression is simply

$$\tilde{r} = \frac{Z_{eff} - 1}{Z_{eff} + 1}. \tag{8}$$

Once we have determined n_{eff} and Z_{eff} according to this prescription, a unique effective permittivity and permeability for the medium are given by

$$\varepsilon_{eff} = \frac{n_{eff}}{Z_{eff}}, \tag{9}$$

$$\mu_{eff} = n_{eff} Z_{eff}. \tag{10}$$

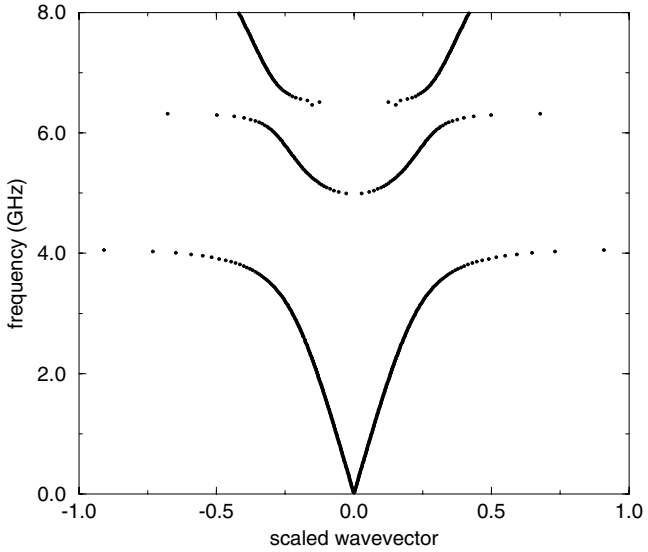

Figure 3. The photonic band structure of a square lattice of cylinders; $\varepsilon = 200$. The cylinder centre-to-centre spacing is 5 mm. The ratio of the cylinder radius to the spacing is 0.4.

Table 1. Microwave properties of BSTO–oxide composite ceramics (taken from [9]).

Oxide content	Frequency (GHz)	Dielectric constant	Loss tangent
30	2.139	646	0.0040
40	1.815	404	0.0042
	3.304	401	0.0051
60	4.581	113	0.0065

A stop band is characterized by an imaginary part of the effective refractive index. Since $n_{eff} = \sqrt{\varepsilon_{eff}\mu_{eff}}$, in the stop-band region we have that the real part of either ε_{eff} or μ_{eff} is negative.

Let us first consider the case of a lossless ferroelectric constituent for our system. This serves to illustrate the perturbative effect of the Mie resonance on the band structure. The results plotted in figure 3 are for a square lattice of cylinders and for propagation along the ΓX direction with dielectric constant $\varepsilon = 200$, cylinder spacing $d = 5$ mm and cylinder-radius-to-spacing ratio of 0.4. The scaled wavevector is the quantity $\beta d/\pi$.

Notice how, away from the stop bands, the bands are dispersing linearly, indicating that we are operating in the effective medium regime. The first stop band is due to the zeroth-order Mie resonance as discussed above. At higher energy we have a more complicated structure as the next resonant mode has a dipolar symmetry and thus there are two possible relative orientations of the fields in adjacent cells in the infinite system.

Below we present results for cylinders with $\varepsilon = 200 + 5\mathrm{i}$. Material parameters such as this are readily attainable as table 1 illustrates [13]. These materials combine the ferroelectric $Ba_{0.6}Sr_{0.4}TiO_3$ (BSTO) with non-electrically active oxide ceramics.

The photonic band structure for our composite is given in figure 4. In order to demonstrate that the assumption that we may consider the dominant branch alone is correct, we have included the lowest two branches. Notice how the imaginary part of the lower branch is always much less than that of the second as desired. The increasing loss in the cylinders

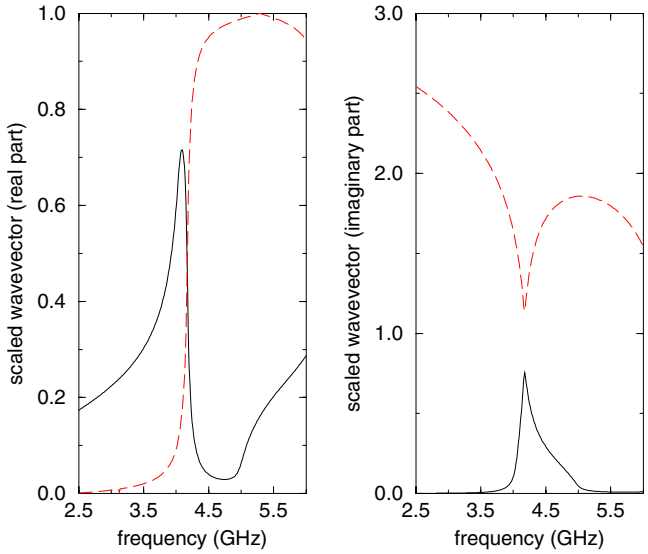

Figure 4. Real parts (left) and imaginary parts (right) of the complex photonic band structure for a square array of cylinders. In each case, the solid curve is the lowest-lying branch and the next branch is the dashed curve. The spacing between cylinders is 5 mm and $\varepsilon = 200 + 5\mathrm{i}$. The ratio of the cylinder radius to the spacing is 0.4.

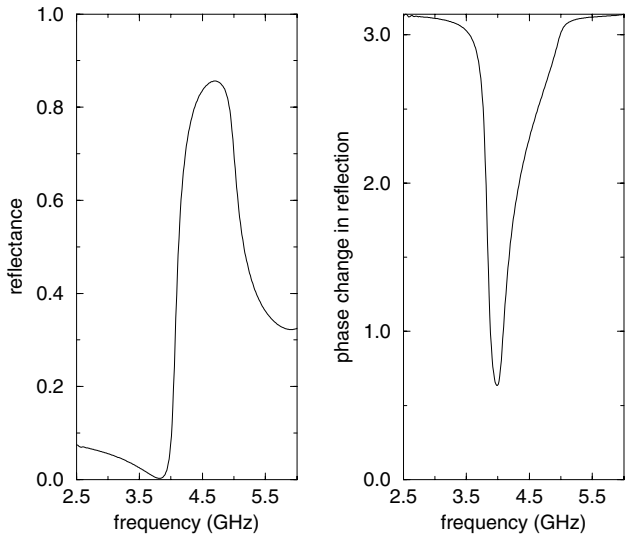

Figure 5. The reflectance (left) and phase change in reflection (right) for the system of figure 4. Ten layer doublings were performed.

serves to average over a finite frequency bandwidth such that a single continuous branch of eigenvalues can be used to determine the effective refractive index.

In figure 5 we present the reflectivity calculated by performing ten layer doublings and the phase change in reflection from the system. At the position of the resonance a stop band exists where almost all of the incident power is reflected. The band of frequency where the

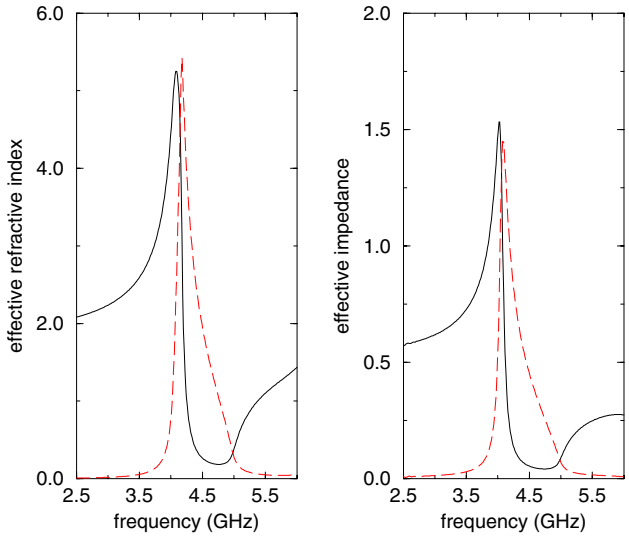

Figure 6. The calculated effective refractive index (left) and effective impedance (right) of the system. The parameters are the same as for figure 4. The solid curve is the real part and the dashed curve is the imaginary part in each case.

reflectivity is close to one is also large. Below this band the dispersion is linear and almost all of the incident radiation is transmitted into the system.

The calculated effective refractive index and effective impedance of the system are presented in figure 6. Consistent with the reflectivity data, at low frequencies we have a primarily real refractive index which develops a large imaginary part as we approach the resonance frequency. In the gap region the refractive index is primarily imaginary, implying strong attenuation of the wave inside the crystal. The width of the stop band is roughly 20% of the band centre frequency. Above the gap region the refractive index is almost zero and as the frequency is increased further we return to the regime of linear dispersion.

The impedance of the surface is defined as

$$Z_{eff} = \frac{E_x}{H_y}. \tag{11}$$

Near the resonance frequency the impedance is large with equal real and imaginary parts. Such a surface has been referred to as a magnetic conductor because even for a large electric field present at the surface the magnetic field is small. Thus the parallel magnetic field has a node at the surface just as the parallel electric field has for normal conductors. It is the appearance of fictitious magnetic poles in the cylinders, because of the Mie resonance, which gives rise to this effect. Since the phase change in reflection from an ideal magnetic conductor is zero, it has been proposed that these artificial materials be employed as base plates to improve the efficiency of antennas [14]. One advantage is that the quarter-wavelength separation between an antenna and a normal-metal base plate is no longer required. In addition, surface waves on the base plate which are a source of interference are no longer supported.

The effective permeability and permittivity of the system are given in figure 7. At low frequencies there is no magnetic activity in the system, $\mu_{eff} = 1$, and the effective permittivity is in good agreement with that calculated using the Maxwell-Garnett theory.

The effective permeability is very strongly dispersive in the vicinity of the Mie resonance. As the frequency is increased, μ_{eff} becomes large and positive with a correspondingly large

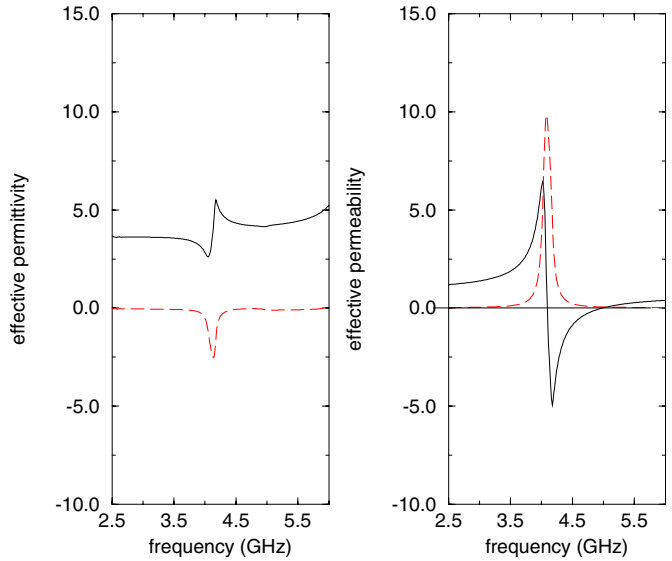

Figure 7. The effective permittivity (left) and effective permeability (right) for the system of figure 4. Again, the solid curves are the real parts and the dashed curves are the imaginary parts.

imaginary part. In the gap region at higher frequency, μ_{eff} is negative and primarily real, approaching the value $1 - f$ as the frequency is increased further. Here f is the filling fraction with dielectric material.

In [5] a microscopic averaging procedure was outlined for calculating μ_{eff} for a 2D system. With this method the permeability is defined as

$$\mu_{eff}^{i,j} = \frac{\langle B_i \rangle}{\mu_0 \langle H_j \rangle}, \tag{12}$$

where the average of B is taken over the 2D unit-cell area and the average of H is taken along a line at the unit-cell boundary parallel to the cylinders. As is the case here, the secret to obtaining a strong effect is to create fields which are as inhomogeneous as possible. The large dielectric constant of our inclusions confines the photons very efficiently leading to a large build-up of fields inside the cylinders. However, notice that the enhanced fields are always parallel to the cylinder surface and therefore do not have a polarization charge associated with them there. This means that the enhanced fields tend to contribute disproportionately to the average of the B-field which is taken over the whole unit cell rather than to the average of the H-field which is taken between cylinders and explains why the permeability approaches a limiting value of $1 - f$ above the resonance frequency.

The plane-wave scattering properties of the single isolated cylinder allow us to write down an approximate analytic expression for the effective permeability of the composite using equation (12). We consider only the contribution of the resonant $m = 0$ mode to the summations of equations (1)–(3) and in calculating the average of the B-field we perform the integration over a circular area of radius r of the same size as the unit cell, i.e. $d^2 = \pi r^2$. Within these approximations the effective permeability of the composite is

$$\mu_{eff} = \frac{2\pi}{d^2} \frac{c_0 \int_0^a J_0(nkr) r \, \mathrm{d}r + \int_a^{d/\sqrt{\pi}} [J_0(kr) - a_0 H_0^{(1)}(kr)] r \, \mathrm{d}r}{J_0(kd/2) - a_0 H_0^{(1)}(kd/2)}. \tag{13}$$

The results are given in figure 8 where we see that the agreement with the values calculated using the transfer matrix method is very good. Both of these calculations are for cylinders with

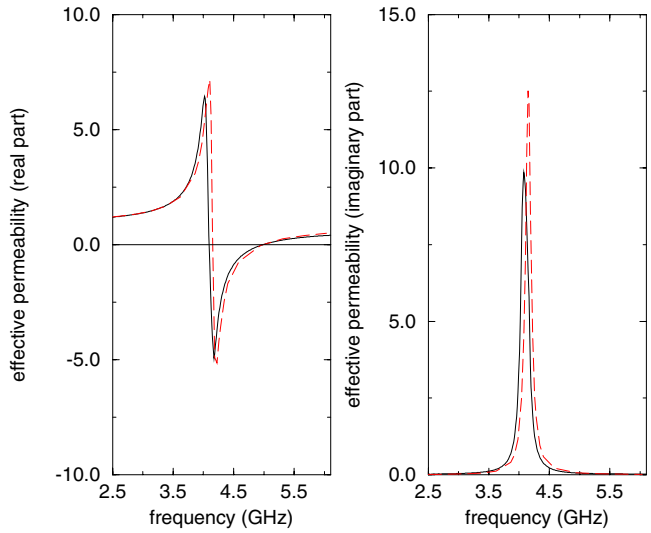

Figure 8. Comparison of the effective permeability calculated using the transfer matrix method (solid curves) and equation (13) (dashed curves).

$\varepsilon = 200 + 5\mathrm{i}$, corresponding to a loss tangent for the inclusions of 0.025. This level of loss can be greatly improved upon, as table 1 illustrates. Calculations of the effective permeability for such low-loss materials suggest that a very large magnetic response, where $\mathrm{Im}\{\mu_{eff}\} \simeq 50$ should be attainable.

Since n_{eff} and Z_{eff} are very nearly proportional, the effective permittivity is not strongly dispersive in this region of frequency. Analogously to equation (12), we can define

$$\varepsilon_{eff}^{i,j} = \frac{\langle D_i \rangle}{\varepsilon_0 \langle E_j \rangle}, \tag{14}$$

where the averages of E and D involve integrals along the boundary of the unit cell. This explains why the behaviour of the average permittivity of the system is so different to that of the average permeability. Somewhat paradoxically, increasing the dielectric constant of the cylinders and the consequent confining effect would serve to reduce the effect of the resonance on the system's ε_{eff}. Note also that the free-space wavelength of the radiation at the resonance frequency is about fifteen unit cells. Thus we can expect the effective medium approximation to be very good in the sense that the system response should not strongly depend on the direction.

4. Applications

The resonant form of our effective permeability is

$$\mu_{eff} = 1 - \frac{f\omega^2}{\omega^2 - \omega_0^2 + \mathrm{i}\gamma\omega}. \tag{15}$$

Thus the filling fraction determines the maximum strength of the effect, given a constant dielectric constant for the cylinders. An isotropic medium with a permeability as above would be desirable. Such a structure would consist of two-dimensional arrays of non-intersecting cylinders oriented parallel to the three cartesian axes. This would necessitate a unit cell four times larger than that considered here, and hence a correspondingly smaller filling fraction and weaker effect. For a given operating range of frequency a larger dielectric constant could be employed along with close packing of cylinders to achieve a 3D structure with the required

properties. Such a structure would support TE-polarized surface waves in the region where $\mu_{eff} < 0$ as well as a bulk magnetic plasmon mode where $\mu_{eff} = 0$. Because of the potential for small losses which these ferroelectric composites provide, they might represent a favourable alternative to metallic structures with an effective permeability as in equation (15).

For the 2D case considered here, or for the isotropic case, combining our structure with interlaced arrays of micron wires raises the possibility of manufacturing a negatively refracting meta-material. The 2D case merely requires the addition of arrayed wires in planes parallel to the xz-plane. Such a structure could be tuned to possess a negative refractive index for p-polarized fields in the microwave region of the spectrum.

A large permeability imparts unusual ac magnetic flux guiding properties to structures. For this reason the 'Swiss-roll' structure [5] was studied in the context of magnetic resonance imaging [15]. The ferroelectric composite can also be expected to possess similar properties at higher frequencies but with the advantages of its inherent tunability and potentially low damping losses. Since any insulating particle will support its own geometrical resonances, we are by no means restricted to the circular inclusions considered here. Ease of fabrication and control of the sizes and material properties of inclusions may be more important.

5. Conclusions

We have presented numerical calculations of the effective permeability and permittivity for a composite structure consisting of dielectric cylinders. Magnetic activity in the composite arose because of the presence of a Mie resonance in the cylinders. Because we took the dielectric constant of the cylinders to be large, the resonance frequency was reached while the free-space wavelength was still many unit cells. A stop band for our composite on the high-frequency side of the resonance was found to be due to a negative effective permeability. Approximate analytic expressions for the averaged fields were also used to calculate the effective permeability of the composite. The agreement with our numerical results was very good.

Acknowledgment

One of the authors, S O'Brien, would like to thank S Anantha Ramakrishna for many helpful discussions.

References

[1] Veselago V G 1968 *Sov. Phys.–Usp.* **10** 509
[2] Pendry J B 2000 *Phys. Rev. Lett.* **85** 3966
[3] Smith D R, Padilla W J, Vier D C, Nemat-Nasser S C and Schultz S 2000 *Phys. Rev. Lett.* **84** 4184
[4] Shelby R A, Smith D R and Schultz S 2001 *Science* **292** 77
[5] Pendry J B, Holden A J, Robins D J and Stewart W J 1999 *IEEE Trans. Microw. Theory Tech.* **47** 2075
[6] Pendry J B, Holden A J, Robins D J and Stewart W J 1998 *J. Phys.: Condens. Matter* **10** 4785
[7] Bohren C F and Huffman D R 1983 *Absorption and Scattering of Light by Small Particles* (New York: Wiley–Interscience)
[8] Ohtaka K and Tanabe Y 1996 *J. Phys. Soc. Japan* **65** 2265
[9] Smith D R, Vier D C, Kroll N and Schultz S 2000 *Appl. Phys. Lett.* **77** 2246
[10] Contopanagos H F, Kyriazidou C A and Merrill W M 1999 *J. Opt. Soc. Am.* A **16** 1682
[11] Garcia-Vidal F J, Pitarke J M and Pendry J B 1997 *Phys. Rev. Lett.* **78** 4289
[12] Pendry J B and MacKinnon A 1992 *Phys. Rev. Lett.* **69** 2772
[13] Sengupta L C 1997 adapted with permission from *Reports on Leading Edge Engineering from the 1996 NAE Symp. on Frontiers of Engineering* (copyright (1997) by the National Academy of Sciences; courtesy of the National Academy Press, Washington, DC)
[14] Sievenpiper D, Zhang L, Broas R F, Alexopoulos N G and Yablonovitch E 1999 *IEEE Trans. Microw. Theory Tech.* **47** 2059
[15] Wiltshire M C K, Pendry J B, Young I R, Larkman D J, Gilderdale D J, and Hajnal J V 2001 *Science* **291** 849